IEEE Access
Multidisciplinary ⋮ Rapid Review ⋮ Open Access Journal

Received September 16, 2019, accepted October 15, 2019, date of publication October 29, 2019, date of current version November 18, 2019.

Digital Object Identifier 10.1109/ACCESS.2019.2949992

Neural Network Sliding Mode Control of Intelligent Vehicle Longitudinal Dynamics

SHAOHUA WANG[1], YIJIA HUI[1], XIAOQIANG SUN[2,3], AND DEHUA SHI[2]
[1]School of Automotive and Traffic Engineering, Jiangsu University, Zhenjiang 212013, China
[2]Automotive Engineering Research Institute, Jiangsu University, Zhenjiang 212013, China
[3]Key Laboratory of Automotive Measurement, Control and Safety, Xihua University, Chengdu 610039, China

Corresponding author: Xiaoqiang Sun (sxq@ujs.edu.cn)

This work was supported in part by the National Natural Science Foundation of China under Grant 51705207 and Grant U1564201, in part by the China Postdoctoral Science Foundation under Grant 2019T120398 and Grant 2017M611728, in part by the Postdoctoral Research Foundation of Jiangsu Province under Grant 1701112B, in part by the Six Talent Peaks Project of Jiangsu Province under Grant GDZB-163, and in part by the Open Research Subject of the Key Laboratory of Automotive Measurement, Control, and Safety (Xihua University) under Grant QCCK2019-002.

ABSTRACT Longitudinal dynamics control is the basis for autonomous driving of intelligent vehicles, which have great significance to the development of intelligent transportation system (ITS). To solve the problems of traditional sliding mode control method when applied to intelligent vehicle longitudinal dynamics, such as large velocity tracking errors, strong chattering phenomenon and so on, a new sliding mode control strategy based on RBF (Radical Basis Function) neural network is presented in this paper. Firstly, a nonlinear mathematical model of the intelligent vehicle longitudinal motion is established by considering the dynamics of the engine, the torque converter, the automatic transmission and the brake system. On the basis of the system model, a variable structure control system with sliding mode is introduced to design a sliding mode variable controller with RBF neural network. This controller can adaptively adjust the switching gain and its stability is proved based on the Lyapunov theory. Finally, the effectiveness of the designed longitudinal velocity control strategy is verified by simulation under typical driving conditions. The simulation results show that the improved control algorithm can effectively suppress chattering, obtain the higher precision and stronger robustness than the traditional sliding mode control. Thus, the longitudinal motion control performance of intelligent vehicles is improved effectively.

INDEX TERMS Intelligent vehicles, intelligent transportation system, longitudinal dynamics control, sliding mode control, RBF neural network.

I. INTRODUCTION

As the development direction of future vehicles and the central part of intelligent transportation system (ITS), intelligent vehicles have been widely concerned by scholars from different countries in recent years [1], [2], [26]. Intelligent vehicles usually can complete one or more driving tasks such as road identification and tracking, obstacle recognition and collision avoidance, vehicle detection and tracking, vehicle lateral and longitudinal motion control, etc. It has great significance to improving the utilization of road network, increasing road capacity, reducing vehicle energy consumption and avoiding accidents as much as possible [3]–[5]. Longitudinal control is not only the basis of autonomous driving of intelligent vehicle but also the main content to realize the active safety of automobiles, and plays a very important role in the intelligent vehicle driving control system [30].

In recent years, with the development of intelligent vehicles and ITS, many scholars have also conducted in-depth research on the vehicle longitudinal control system. For example, a direct control structure was used by A. Ferrara *et al.* to design the second-order sliding mode longitudinal control strategy based on least sensors, with an acceleration observer constructed to estimate the vehicle acceleration [4]. Based on the output recursive cerebellum model, Y. Peng designed a vertical adaptive inversion control strategy for intelligent vehicles, which had strong robustness to guarantee the stability of the closed-loop system [7]. Y. N. Li *et al.* proposed the parameters self-tuning fuzzy-PID longitudinal controller to decrease the overshoot, enhance the capacity of anti-dynamic disturbance and have certain robustness. [8]. Palhares *et al.* used the system identification method to establish the longitudinal dynamic model and compensated

The associate editor coordinating the review of this manuscript and approving it for publication was Yonghao Gui.

This work is licensed under a Creative Commons Attribution 4.0 License. For more information, see http://creativecommons.org/licenses/by/4.0/

the nonlinear characteristics of the system with the inverse dynamic model [9].

According to these published literatures, most scholars used fuzzy control [10], [29], model predictive control [11], [24], and robust control [12] to regulate the longitudinal velocity of the vehicles and improve the accuracy of speed tracking. However, the disadvantage of these control methods is that they require specific models and complex structures. The vehicle longitudinal dynamics control system is a complex nonlinear system whose characteristics are difficult to be accurately described by linear models. For nonlinear systems with uncertainty and external disturbances, sliding mode control (SMC) is one of the important methods to design longitudinal velocity controllers during these years [13], [14], [25]. However, the gain in the sliding mode control will cause high frequency chattering in the control system. Thus, how to reduce the high frequency chattering phenomenon has become an important quality factor of sliding mode control method.

Compared with the traditional sliding mode control, the non-singular terminal sliding mode control has the advantages of fast dynamic response speed, limited time convergence, elimination of chattering and high steady-state tracking accuracy, which is suitable for longitudinal velocity control [15]–[18]. Since neural network has strong adaptiveness, fault tolerant performance, and approximation characteristics [19], [20], the unknown parameters of the controlled object model can be approximated by this method. An adaptive neural network sliding mode control (ANN-SMC) law designed by J. Guo *et al.* to enhance control effect of Speed tracking control [21]. In different neural network control strategies, RBF neural network has a simple structure and can approximate any nonlinear function. It converges quickly and has the ability to implement real-time control in complex environments [22]. P. Hang *et al*. designed an improved adaptive sliding mode control (ASMC) algorithm using Radial Basis Function (RBF) neural network, which has smaller tracking error and better disturbance rejection performance than SMC [22]. Based on these advantages, a non-singular terminal sliding mode control strategy based on RBF (Radical Basis Function) neural network is proposed to regulate longitudinal velocity in this paper.

The major purpose of this paper is to provide an accurate and consistent acceleration tracking control of vehicle longitudinal speed. Based on the non-singular terminal sliding mode control (NTSMC) and RBF neural network, the control algorithm is designed to get approximately homogeneous and linear node dynamics, which can not only make the system have the characteristics of strong robustness and fault tolerance, but also reduce system chattering problem effectively.

The main contributions of this paper are as follows:

1) The non-singular terminal sliding mode control algorithm is designed to get the higher tracking accuracy and the faster dynamic response than the traditional sliding mode control.

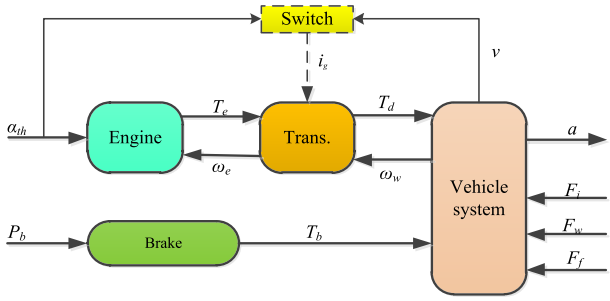

FIGURE 1. Sketch of vehicle longitudinal dynamics.

2) An adaptive algorithm combining neural network and terminal sliding mode control is designed, which can eliminate the system chattering and achieve stable sliding mode control without the accurate model of the object.

The rest of this paper is organized as follows: Section II describes the vehicle model for control. Section III designs the RBF-NTSMC controller and proves its stability. Section IV shows the simulation results and compares them with traditional sliding mode controllers. Finally, Section V gets the conclusions of this paper.

II. SYSTEM MODEL

In this paper, the assumptions for vehicle longitudinal dynamics models are made as follows [5].

1) The dynamics in intake manifold and chamber combustion are neglected, and the overall powertrain dynamics are lumped into a first-order inertial transfer function.

2) The vehicle runs on dry alphabet roads with high road–tire friction, and the tire longitudinal slip is neglected.

3) The vehicle body is considered to be rigid and symmetric, without vertical motion, yaw motion, and pitching motion.

4) The hydraulic braking system is simplified to be a first-order inertial transfer function without pure time delay.

Under the condition of these assumptions, the power train system of the intelligent vehicle adopts the design of front engine and rear wheel drive [36], [37]. The vehicle for control is a passenger car with a gasoline engine, a torque converter, a four-speed automatic transmission and a braking system. Fig. 1 shows the powertrain dynamics. The inputs of the system are the throttle angle α_{th} and the brake pressure P_b. The outputs include longitudinal acceleration a, vehicle velocity v and other measurable variables.

A. THE ENGINE MODEL

Ignoring the influence of the throttle lag time and the torsional stiffness of the drive shaft on the engine performance, the engine steady-state output torque T_e can be determined by the engine speed ω_e and the throttle opening α_{th} by the following formula.

$$T_e = Eng\,(\alpha_{th}, \omega_e) \tag{1}$$

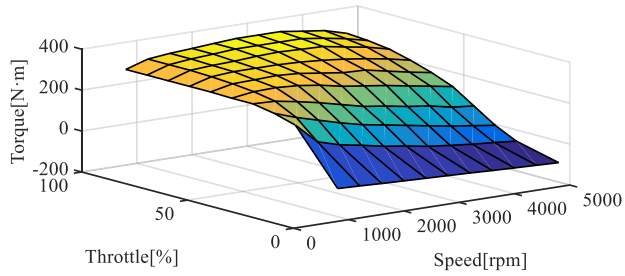

FIGURE 2. Engine torque map.

From the data of the engine, the engine torque characteristic function can be obtained by Look-up Table model in the MATLAB simulation system. The model can be used to represent the relationship among output torque T_e, the engine speed ω_e and the throttle opening α_{th}. The characteristics are shown in Fig. 2.

According to the relationship between the engine and the torque converter, it is obtained that:

$$J_e\dot{\omega}_e = T_e - T_p \tag{2}$$

where T_p is the pump torque of the torque converter(TC), J_e is the inertia of fly wheel.

According to the above assumptions, the engine torque characteristic function is combined with a first-order inert phase to represent the dynamic characteristics of the engine output torque:

$$f_e\left(\alpha_{th}, \omega_e\right) = T_e + \tau_e \cdot \dot{T}_e \tag{3}$$

where τ_e represents the first-order inertia link constant.

According to (2) and (3), the first-order inertial engine simplified model dynamics is obtained:

$$\frac{f_e\left(\alpha_{th}, \omega_e\right) - \left(T_p + \tau_e \cdot \dot{T}_p\right)}{J_e} = \dot{\omega}_e + \tau_e \cdot \ddot{\omega}_e \tag{4}$$

B. TORQUE CONVERTER AND AUTOMATIC TRANSMISSION MODEL

The torque converter characteristics include two parts: torque characteristics and capacity characteristics, whose characteristics are shown in Fig. 3(a) and Fig. 3(b). The torque characteristics and capacity characteristics are expressed as follows:

$$\frac{T_t}{T_p} = \tau\left(\frac{\omega_t}{\omega_p}\right) \tag{5}$$

$$\frac{T_p}{\omega_p^2} = K_{tc}\left(\frac{\omega_t}{\omega_p}\right) \tag{6}$$

The torque converter pump torque expression can be obtained from (6):

$$T_p = K_{tc}\left(\frac{\omega_t}{\omega_p}\right) \cdot \omega_p^2 \tag{7}$$

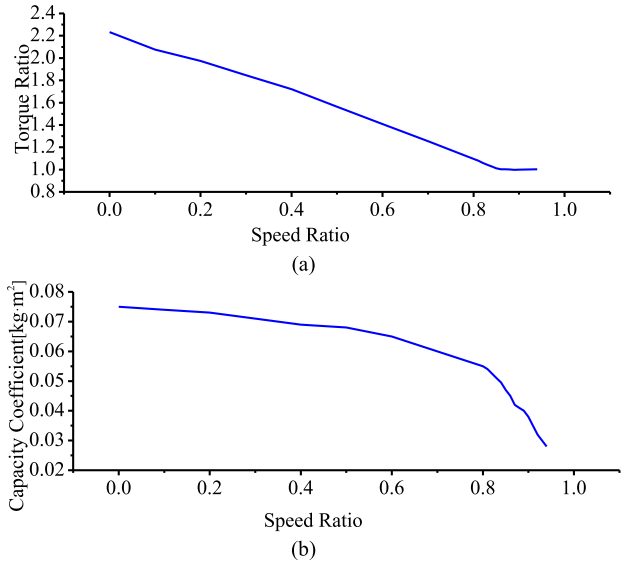

FIGURE 3. Characteristics of TC. (a) Torque ratio. (b) Capacity coefficient.

Bring (7) into (5) to obtain the torque converter turbine torque expression:

$$T_t = K_{tc}\left(\frac{\omega_t}{\omega_p}\right) \cdot \omega_p^2 \cdot \tau\left(\frac{\omega_t}{\omega_p}\right) \tag{8}$$

where τ is the torque ratio factor, K_{tc} is the torque ratio of torque converter, T_p is the pump wheel torque, and T_t is the turbine torque.

In the simulation, the finite state machine theory is used to describe the gear shifting behavior of the automatic transmission, and the gear shifting model is established by Stateflow module in MATLAB. Automatic transmission gear shift rules are related to the throttle percentage α and the automatic transmission output speed ω_t.

In this paper, the intelligent vehicle adopts the four-speed automatic transmission. The switching logic of automated transmission is shown in Fig. 4.

C. BRAKE MODEL

The front and rear brake systems use disc brakes. Using response lag time τ_b to describe the time lag phenomenon during braking, the mathematical model of the brake is described as follows:

$$T_b = \frac{2}{\tau_b s + 1}\mu_{br}A_{br}R_{br}p_{br} \tag{9}$$

where T_b is the vehicle braking torque, μ_{br} is the brake friction factor, A_{br} is the brake disc friction area, R_{br} is the braking force radius, and P_{br} is the brake pressure.

D. LONGITUDINAL DYNAMICS ANALYSIS OF VEHICLES

Suppose that the vehicle is driving on a sloped road and the vehicle itself is regarded as a rigid body. The forces on the vehicle are shown in Fig. 5. The tire stress point on each axle is subject to the longitudinal direction force and the normal

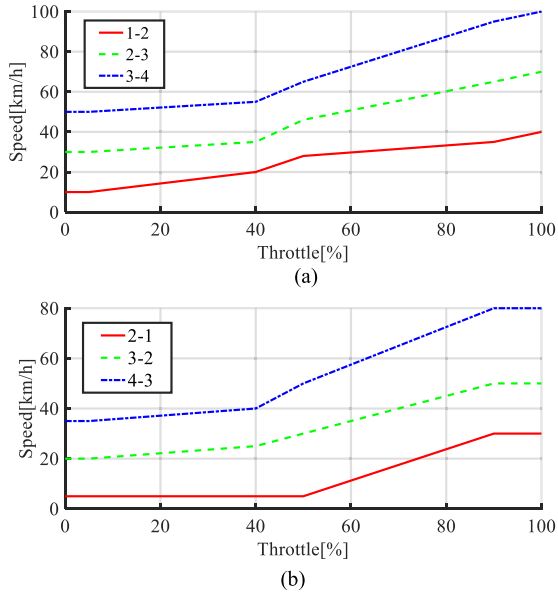

FIGURE 4. Switching logic of automated transmission. (a)Shift-up rule. (b)Shift-down rule.

direction force. Other external forces acting on the body include air resistance, rolling resistance and gravity [33].

According to Newton's second law, the equilibrium equation along the x-axis of the vehicle's longitudinal direction can be calculated by:

$$F_t = F_f + F_w + F_j + F_b \tag{10}$$

The mathematical model of vehicle longitudinal dynamics is:

$$\begin{aligned} F_t &= \frac{T_d}{r} = \frac{T_0 i_0 \eta_t}{r} \\ F_b &= k_b p_b \\ F_j &= \delta m \dot{v} \\ F_w &= \frac{1}{2} C_D A \rho u^2 \\ F_f &= mgf\sin(\theta) \\ \delta m \dot{v} &= \frac{T_0 i_0 \eta_t}{r} - k_b p_b - mgf\sin(\theta) - \frac{1}{2} C_D A \rho u^2 \end{aligned} \tag{11}$$

where F_t is driving force, F_b is brake force, F_j is acceleration resistance, F_w is the air resistance, F_f is the rolling resistance, δ is the vehicle's rotational mass conversion coefficient, m is the total mass of the vehicle; v is the absolute speed, i_0 is the final drive ratio, k_b is the brake pressure proportionality factor, p_b is the brake pressure, f is the rolling resistance coefficient, θ is the ramp angle, C_D is the air resistance, A is the windward area, ρ is the air density and u represents relative speed.

III. CONTROL STRATEGY

The intelligent vehicle longitudinal velocity control system is an integrated control system consisting of acceleration target control and servo switching control. The structure of the control system is shown in Fig. 6.

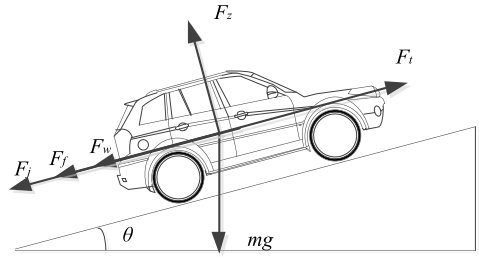

FIGURE 5. Longitudinal dynamic schematic of vehicles.

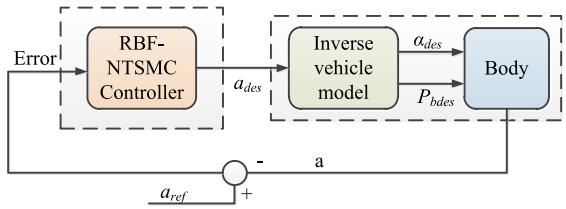

FIGURE 6. Control configuration for vehicle acceleration tracking.

The controller includes throttle controller and brake controller. According to different characteristics of throttle/brake control, the throttle/brake RBF neural network non-singular terminal sliding mode control system is separately designed.

A. DESIGN OF NON-SINGULAR TERMINAL SLIDING MODE CONTROLLER

In this paper, the relative speed error of vehicles is an important index for evaluating the longitudinal velocity control system [27]. In order to improve the control accuracy of the model, the relative acceleration error of the workshop is used as another indicator of the control system. Under these circumstances, define the variable parameters of the upper non-singular terminal sliding mode controller as:

$$e = v_0 - v_{ref} \tag{12}$$

$$\dot{e} = a_0 - a_{ref} \tag{13}$$

where e and $\dot{e}$ respectively represent speed error and acceleration error, v_0 is the tracking vehicle speed, a_0 is the tracking vehicle acceleration, v_{ref} is the reference speed, and a_{ref} is the reference acceleration.

From (11), according to the vehicle driving dynamics equation, the desired acceleration a_{des} can be defined as:

$$a_{des} = \dot{v}_{des} = \frac{T_{edes} i_0 \eta_t}{\delta m r} - \frac{k_b p_{bdes}}{\delta m} - \frac{mgfsin(\theta)}{\delta m} - \frac{C_D A \rho v_{ref}^2}{2\delta m} \tag{14}$$

The derivation is defined as:

$$\ddot{v}_{des} = A_1 \dot{T}_{edes} - B_1 \dot{p}_{bdes} - B_2 v_{ref} \tag{15}$$

where T_{edes} is the engine desired torque, and p_{bdes} is the desired brake pressure.

The engine desired torque is selected as the control variable. The purpose of the control is to make the desired speed follow the change of the vehicle speed. According to the

theory of sliding mode control, the sliding mode switching surface of adaptive cruise control is designed as:

$$s = e + \rho \cdot \dot{e}^{p/q}, \quad \rho > 0,\ 1 < p/q < 2 \tag{16}$$

Derivation of the sliding surface can be obtained:

$$\dot{s} = \dot{e} + \rho \cdot (p/q)\dot{e}^{p/q-1}\ddot{e} \tag{17}$$

From formula (17), it can be found that when the state variable of the system is closer to the sliding surface, at this point, the convergence speed of the state variable is not different from the linear sliding mode surface. They all decay exponentially. However, when the system is far away from the sliding surface, the advantages of non-singular fast terminal sliding mode will be reflected, the state variable of the system will be determined by $\dot{e}$. During this time, the convergence speed of the system will be greatly improved compared with the traditional linear sliding surface.

Bringing (15) to (17) leads to the conclusion:

$$\dot{s}=\dot{e}+\rho \cdot (p/q)\dot{e}^{p/q-1}\left[\ddot{v}_0-(A_1\dot{T}_{edes}-B_1\dot{p}_{bdes}-B_2v_{ref})\right] \tag{18}$$

Define L_n as:

$$L_n = A_1\dot{T}_{edes} - B_1\dot{p}_{bdes} \tag{19}$$

Bringing L_n into (18):

$$\dot{s} = \dot{e} + \rho \times (p/q)\dot{e}^{p/q-1}\left(\ddot{v}_0 - L_n + B_2v_{ref}\right) \tag{20}$$

In order to make the movement point of the control system return to the nonlinear sliding surface quickly and correctly, the switching control rate is defined as follows:

$$Q_u = k\mathrm{sgn}(s) + \mu s \quad k > 0,\ \mu > 0 \tag{21}$$

In the formula, k and μ are switching gains, and the value should be large enough. Q_u=$[Q_{11}, Q_{12}]^T$, $Q_u \in R^{2\times 1}$, $sgn(s)$ is the singum function, defined as follows:

$$\mathrm{sgn}(s) = \begin{cases} +1 & s_{i1}\ (i = 1, 2) > 0 \\ -1 & s_{i1}\ (i = 1, 2) < 0 \end{cases} \tag{22}$$

Non-singular terminal sliding mode control law L_u can be defined as:

$$L_u = \ddot{v}_0 + B_2v_{des} + \rho \cdot (p/q)\dot{e}^{2-p/q} + Q_u \tag{23}$$

The Lyapunov function $V_u(s)$ and the first derivative of $V_u(s)$ versus time are separately shown in the following two equations:

$$V_u(s) = \frac{1}{2}s^Ts \tag{24}$$

$$\dot{V}_u(s) = s^T\dot{s} \tag{25}$$

Bring the design control law (23) into (20) to simplify as:

$$\dot{V}_u(s) = s^T \cdot \rho \cdot (p/q)\dot{e}^{p/q-1}\,(-Q_u) \tag{26}$$

From (26), it is known that $\dot{V}_u < 0$, p, q are odd number, $1 < p/q < 2$. Therefore, $s^T \cdot \rho \cdot (p/q)\dot{e}^{p/q-1} > 0$.

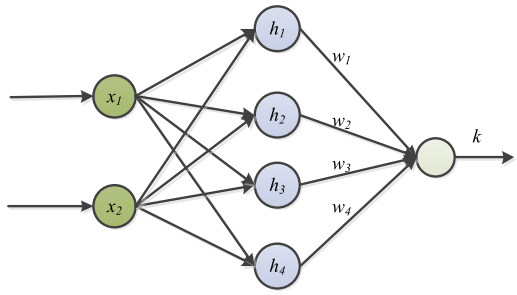

FIGURE 7. The structure of RBF neural network.

Because $\dot{V}_u < 0$, the Lyapunov stability judgment is satisfied. By designing a suitable control law, the linear sliding mode arrives and remains zero in a limited time, $\dot{V}_u = 0$. At this time, the linear sliding mode variable s enters the sliding mode motion state. The error state variables e and $\dot{e}$ enter the sliding mode state to achieve system state convergence.

Based on the sliding mode control algorithm, the input value u of the control system is obtained from the designed control law, which is the desired acceleration a_{des} of demand. These above meet the design requirements, and prove that the proposed NTSMC control approach is feasible.

B. DESIGN OF RBF NEURAL NETWORK CONTROLLER

It is obvious that the sliding mode control algorithm has better robust performance than other traditional control algorithms [31]. This is mainly because the sliding mode control system can design the sliding mode surface according to the requirements of the controlled object. But the sliding mode control also has the disadvantage of chattering problem caused by its own characteristics, which would severely limit its development prospects.

The RBF neural network control has the characteristics of universal function approximation and the ability of adaptive adjustment. If it is combined with terminal sliding mode control, the joint control can greatly simplify the parameter selection process while ensuring the robustness of the system. Therefore, the controller is further designed by means of RBF neural network structure and the switching gain k of the sliding mode controller is adaptively adjusted to reduce the chattering of the system and save the adjustment time of the sliding mode variable controller. The RBF neural network designed in this paper has two inputs, four hidden layer nodes, and one output. The structure of the RBF neural network is shown in Fig. 7.

The input of the RBF neural network is $x = [x_1x_2]^T = [s\dot{s}]^T$ and the output of the RBF neural network is:

$$u(t) = w \cdot h = \left|\sum_{j=1}^{4} w_j \cdot h_j\right| = k \tag{27}$$

where $w = [w_1, w_2, w_3, w_4]^T$ is the weight vector of RBF neural network, $h = [h_1, h_2, h_3, h_4]^T$ is the radial basis vector of RBF neural network.

The radial basis vector h_j is the Gaussian function:

$$h_j = \exp(-\frac{\|x - c_j\|^2}{2b_j^2}) \tag{28}$$

In the formula, $c_j = [c_1, c_2, c_3, c_4]$ is the central vector of the network node and $b_j = [b_1, b_2, b_3, b_4]$ is the base width vector of the network.

According to the sliding mode control principle, when the control target is $s\dot{s} \to 0$, the weight adjustment index of the RBF neural sliding mode is: $E = s(t)\dot{s}(t)$.

Therefore, the weight parameter change can be defined as:

$$\begin{aligned} dw_j &= -\eta \frac{\partial E}{\partial w_j(t)} = -\eta \frac{\partial s(t)\dot{s}(t)}{\partial w_j(t)} \\ &= -\eta \frac{\partial s(t)\dot{s}(t)}{\partial k} \frac{\partial k}{\partial w_j(t)} \quad \eta > 0 \end{aligned} \tag{29}$$

Because of

$$\frac{\partial s(t)\dot{s}(t)}{\partial k} = s(t)\frac{\partial \dot{s}(t)}{\partial k} = -bs(t) \tag{30}$$

it can be got that:

$$\frac{\partial k}{\partial w_j(t)} = \exp(-\frac{\|x - c_j\|^2}{2b_j^2}) \tag{31}$$

where b and x are the system input parameters.

Based on (29) and (30), it can be obtained that:

$$\begin{aligned} dw_j &= \eta \cdot b \cdot s(t) \cdot \exp(-\frac{\|x - c_j\|^2}{2b_j^2}) \\ &= \eta \cdot b \cdot s(t) h_j \end{aligned} \tag{32}$$

The width parameter variation of the Gaussian function obtained by (32) is:

$$db_j = -\eta \frac{\partial E}{\partial b_j} = \eta \cdot b \cdot s(t) w_j h_j \frac{\|x - c_j\|^2}{b_j^3} \tag{33}$$

The parameter of the hidden node neuron center node is:

$$dc_{ji} = -\eta \frac{\partial E}{\partial c_j} = \eta \cdot b \cdot s(t) w_j h_j \frac{x - c_{ji}}{b_j^2} \tag{34}$$

The RBF neural network weight adjustment algorithm established in this paper can be expressed as follows:

$$w_j(t) = w_j(t-1) + dw_j(t) + \eta(w_j(t-1) - w_j(t-2)) \tag{35}$$

$$b_j(t) = b_j(t-1) + db_j(t) + \eta(b_j(t-1) - b_j(t-2)) \tag{36}$$

$$c_j(t) = c_j(t-1) + dc_j(t) + \eta(c_j(t-1) - c_j(t-2)) \tag{37}$$

C. INVERSE VEHICLE LONGITUDINAL DYNAMIC

When the vehicle is in steady driving state, there is a corresponding relationship among longitudinal driving speed, the engine's torque and speed. According to the expected acceleration a_{des} obtained by the upper controller, the inverse longitudinal dynamics model converts the expected acceleration input by the inferior control system into throttle percentage and braking pressure to control vehicle motion [28].

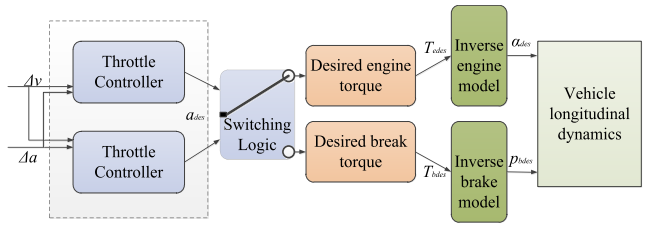

FIGURE 8. Inverse model for vehicle longitudinal dynamics.

The structural diagram of inverse longitudinal dynamic model is shown in Fig. 8.

The system is switched between the engine torque output control and the brake torque control. If the system is switched to engine torque output control, it is necessary to calculate the desired throttle percentage according to the desired acceleration. Besides, the calculation of desired engine torque and the inverse engine model are required during this period. Ignoring the mass conversion of the rotating parts of the vehicle, the motion equation of the vehicle is manifested as follows:

$$m\dot{v}_{des} = F_t - F_b - F_f(v) \tag{38}$$

where F_t is the driving force of the engine acting on the vehicle, F_b is the braking force of the braking action, and $F_f(v)$ is the sum of other resistances such as rolling resistance, wind resistance and engine drag resistance.

According to the assumptions of vehicle longitudinal dynamics system model established above, without considering the elastic deformation of the tire and the drive train, the driving force can be expressed as:

$$F_t = \frac{T_e \cdot \tau\left(\frac{\omega_t}{\omega_e}\right) \cdot i_0 R_g \eta_t}{r} \tag{39}$$

Set

$$k_t = \frac{\tau\left(\frac{\omega_t}{\omega_e}\right) \cdot i_0 R_g \eta_t}{r} = \frac{\tau\left(\frac{v i_0 R_g}{r\omega_e}\right) \cdot i_0 R_g \eta_t}{r} \tag{40}$$

In the process of vehicle motion and vehicle longitudinal dynamics model simulation, k_t is a real-time observation. Substitute equation (40) into equation (39), and get:

$$F_t = T_{des} \cdot k_t \tag{41}$$

Based on (38) $\sim$ (40), the desired engine torque T_{des} can be calculated by

$$T_{des} = \frac{m\dot{v}_{des} + F_f(v)}{k_t} \tag{42}$$

According to the desired engine torque and engine speed, the desired throttle percentage can be obtained by means of the inverse engine model. The inverse engine model is showed as follows:

$$\alpha_{des} = Eng^{-1}(T_e, \omega_e) \tag{43}$$

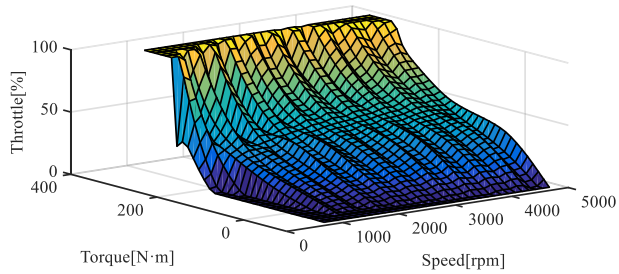

FIGURE 9. Throttle opening characteristics of engine.

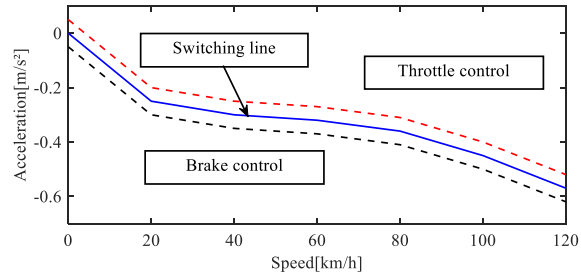

FIGURE 10. Switching line between throttle and brake controls.

Using the data shown in Fig. 3, the inverse engine torque characteristic function, which can be obtained from the output torque of the engine and the engine speed to find the throttle percentage, is shown in Fig. 9.

After the switching between engine torque output and brake control, if the system is switched to the brake control, the desired braking pressure needs to be calculated according to the desired acceleration [38], [39]. During this period, the inverse braking system model needs to be established. Based on the relationship between the braking force and the braking pressure, the desired braking force and the inverse braking system model can be determined by:

$$P_{des} = \frac{\left|m\dot{v}_{des} + F_f(v)\right|}{k_{Kd}} \tag{44}$$

where P_{des} is the desired braking pressure, and k_{Kd} is the braking pressure ratio coefficient.

D. ACCELERATION/BRAKE SWITCHING

In terms of ride comfort and reliability of the corresponding components of the vehicle [32], frequent switches between engine torque control and braking torque control should be avoided during the running of vehicles, because frequent control the throttle and brake at the same time may cause system oscillations and performance conflicts. Therefore, the switching line of the throttle/brake control should be determined according to the desired acceleration [34], [35]. The line is defined as the longitudinal acceleration a_0 of the vehicle when the throttle percentage is minimum and is determined by the engine reverse torque, the gear ratio of each gear, the rolling resistance and the windward resistance. The specific formula is as follows:

$$a_0(v) = \frac{\frac{F_{t0}}{r} - mgf - \frac{1}{2}C_D A\rho u^2}{\delta \cdot m} \tag{45}$$

where F_{t0} is the driving force for the full throttle closing. The switching logic is defined as follows:

$$\begin{aligned} a_{des} &> a_0(v) \quad \text{Engine control} \\ a_{des} &\leq a_0(v) \quad \text{Brake control} \end{aligned} \tag{46}$$

Therefore, the switching line is actually equal to the deceleration when coasting, as shown in Fig. 10.

TABLE 1. Nominal parameters of vehicle model.

Symbol	Meaning	Nominal value
m	vehicle equipment quality	1770 kg
r	wheel radius	0.28 m
C_d	wind resistance coefficient	0.38
A	equivalent windward area	1.87 m^2
i_0	main reducer transmission ratio	4.5
i_g	gear ratio of transmission	[2.27, 1.44, 1.00, 0.74]
f	rolling resistance coefficient	0.03
η_t	mechanical efficiency of driveline	0.90
k_{Kd}	brake pressure ratio coefficient	1.2
ρ	air density	1.2258
J_e	inertia of fly wheel	0.15 kg·m^2

To avoid frequent switching between engine control and brake control, a hysteresis layer is introduced near the switching surface, and the switching logic is redefined as follows:

$$\begin{aligned} a_{des} - a_0(v) &> h \quad \text{Engine control} \\ a_{des} - a_0(v) &\leq -h \quad \text{Brake control} \end{aligned} \tag{47}$$

In this system, the hysteresis layer $h = 0.05$ m/s^2.

IV. SIMULATION RESULTS AND ANALYSES

In this section, the simulation results of the vehicle longitudinal tracking control are analyzed to demonstrate the validity of the proposed RBF-NTSMC control system. The model uncertainties and external disturbances are considered as the random numbers, and the vehicle parameters are listed in Table 1.

To reflect the control effect, a sliding mode controller (SMC) controller is designed at the same time to compare with the RBF-NTSMC controller.

According to (17) and (18), the sliding mode switching surface of longitudinal velocity control is:

$$s = e + \lambda \int_0^t e dt \tag{48}$$

When $\lambda > 0$, the control law is designed as follows:

$$\dot{s} = v_{des} - \dot{v}_{ref} + \lambda(v_{ref} - v_0) \tag{49}$$

$$\dot{s} = -\varepsilon \mathrm{sgn}(s) - ks \; \varepsilon > 0, k > 0 \tag{50}$$

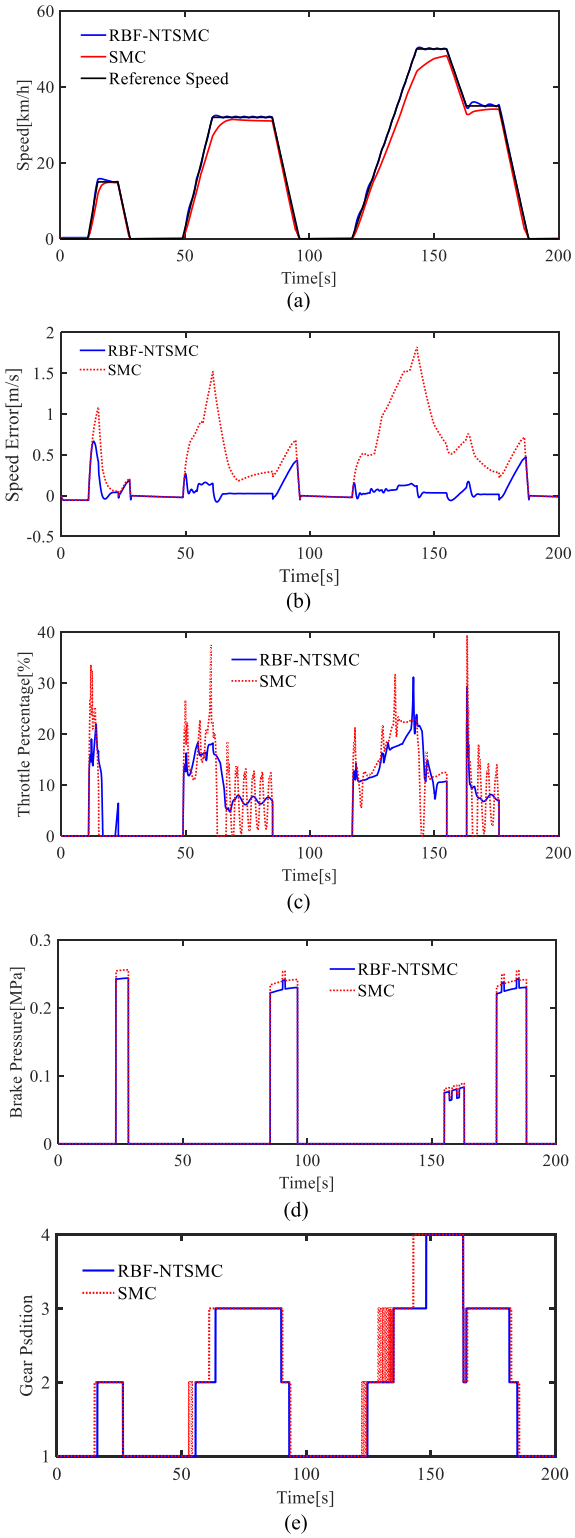

FIGURE 11. Simulation results under NEDC. (a) Vehicle speed. (b) Speed error. (c) Throttle percentage. (d) Brake pressure. (e) Gear position.

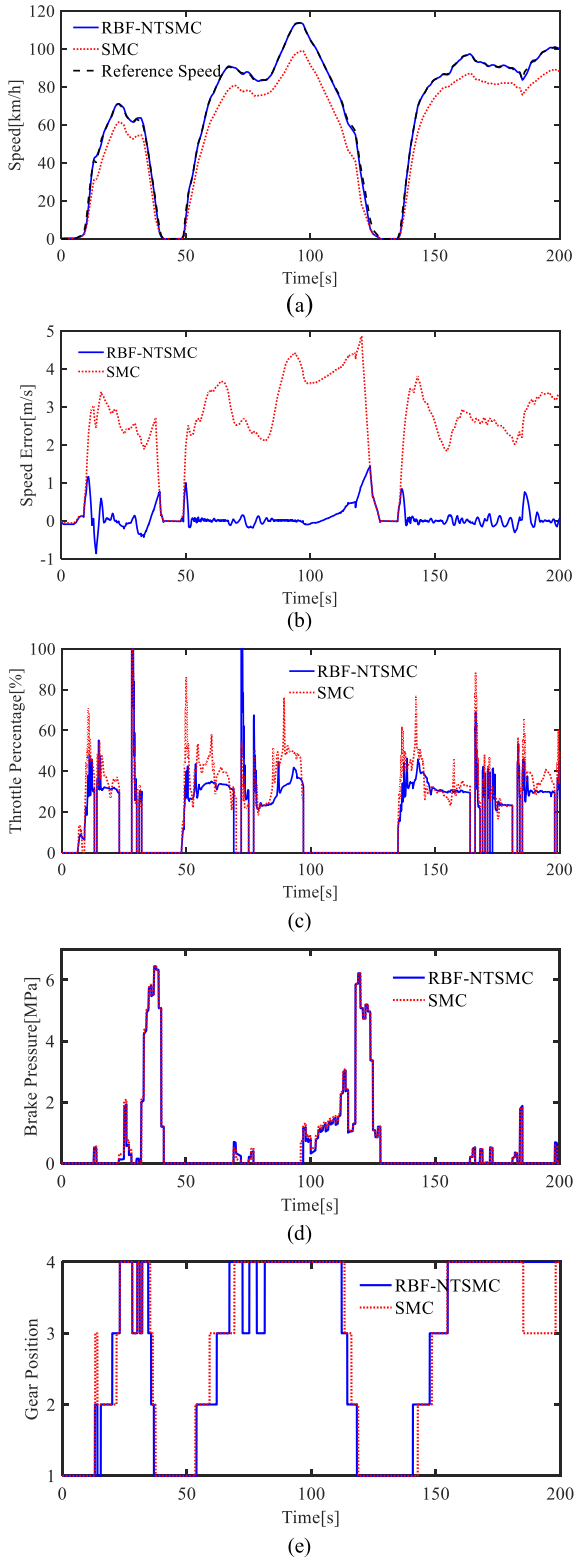

FIGURE 12. Simulation results under SFTP. (a) Vehicle speed. (b) Speed error. (c) Throttle percentage. (d) Brake pressure. (e) Gear position.

According to (49) and (50), the sliding mode controller is described as:

$$v_{des} = \dot{v}_{ref} - \lambda e - \varepsilon \mathrm{sgn}(s) - ks \tag{51}$$

The simulation is performed with two reference vehicle speeds respectively. The simulation time is set to 200s, and the simulation results are shown in Fig.11-12.

First, neglecting the grade of ground, based on MATLAB platform, the New European Driving Cycle (NEDC) simulation results of RBF-NTSMC controller and SMC controller are contrastively showed in Fig. 11.

The responses of longitudinal velocity, the speed and speed error, are respectively shown in Fig. 11(a) and Fig. 11(b). It is obviously that the velocity controlled by the proposed RBF-NTSMC approach is in better consistent with the desired tracking speed than SMC. The most steady-state speed error of these two controllers is 1.67 m/s. Compared with SMC control, the proposed RBF-NTSMC control not only obtains the better tracking precision, but also has the smaller oscillation and less overshoot.

Second, the simulation is carried out under the SFTP (Supplement Federal Test Procedures) condition with relatively rapid speed changing. Similarly, the vehicle performs three rapid accelerations and three rapid decelerations within 200s. The corresponding simulation results are shown in Fig. 12.

As shown in Fig.11(b) and Fig.12(b), compared with SMC control, the performance in average speed error can be reduced by 77.1%, and 95.3% respectively.

Fig. 11(c) shows that the proposed RBF-NTSMC control can effectively reduce the system oscillation caused by the SMC control and make the throttle output smoother under throttle control than SMC control.

Fig. 11(e) shows the performances of gear position change under the two different controllers. Compared with the SMC control, the gear switching is more stable under the proposed RBF-NTSMC control. Especially in the range of 130-140 seconds, gear switching under the SMC control is too frequent to affect driving safety and driving stability seriously.

It can be seen from Fig.11 and Fig.12 that under the proposed RBF-NTSMC control the speed tracking can always be consistent with the desired tracking speed. But, under the traditional SMC control, the speed doesn't track well, especially at the relative high and steady-speed state, its speed error is larger than that of the low-speed condition, and the maximum is up to 4.38 m/s. As shown in Fig.11 (b) and Fig.12 (b), under NEDC and SFTP conditions, the performance in average speed error of the proposed RBF-NTSMC control can be reduced 77.1% and 95.3% respectively.

For brake control, Fig. 11(d) and Fig. 12(d) show that the effect of the proposed RBF-NTSMC control is basically the same as that of SMC. It is concluded that the optimization of RBF-NTSMC control mainly focuses on throttle control.

From Fig.12 (e), the gear switching performance of the proposed RBF-NTSMC control is also better than that of the SMC control.

V. CONCLUSION

In this paper, a new method of longitudinal dynamics control of intelligent vehicle is proposed. Bases on the traditional vehicle dynamics model, the RBF-NTSMC control approach is designed to realize the speed tracking of the vehicle under different working conditions. In order to realize this control, the model which can truly reflect the nonlinear time-varying characteristics of the vehicle longitudinal dynamics is built and the control algorithm is applied to control throttle percentage and brake pressure. The simulation results prove the effectiveness and the potential of the proposed control strategy. Compared with traditional SMC, the RBF-NTSMC can not only effectively reduce relative speed errors and throttle response during longitudinal speed control, but also reduce the chattering of the system. In a word, the proposed RBF-NTSMC algorithm improves the tracking ability and adaptability of intelligent vehicles under various driving conditions.

REFERENCES

[1] A. Y. S. Lam, Y.-W. Leung, and X. Chu, "Autonomous-vehicle public transportation system: Scheduling and admission control," *IEEE Trans. Intell. Transp. Syst.*, vol. 17, no. 5, pp. 1210–1226, May 2016.

[2] R. Kala and K. Warwick, "Intelligent transportation system with diverse semi-autonomous vehicles," *Int. J. Comput. Intell. Syst.*, vol. 8, no. 5, pp. 886–899, 2015.

[3] S. Huang and W. Ren, "Autonomous intelligent vehicle and its performance in automated traffic systems," *Int. J. Control*, vol. 72, no. 18, pp. 1665–1688, Nov. 2010.

[4] G. Wang, M. Yin, and C. Liang, "Measurement system of tire footprint geometric parameters based on image processing," *J. Jiangsu Univ. Nat. Sci.*, vol. 38, no. 2, pp. 139–143, Mar. 2017.

[5] X. Sun, Y. Cai, S. Wang, X. Xu, and L. Chen, "Optimal control of intelligent vehicle longitudinal dynamics via hybrid model predictive control," *Robot. Auton. Syst.*, vol. 112, pp. 190–200, Feb. 2019.

[6] A. Ferrara and P. Pisu, "Minimum sensor second-order sliding mode longitudinal control of passenger vehicles," *IEEE Trans. Intell. Transp. Syst.*, vol. 5, no. 1, pp. 20–32, Mar. 2004.

[7] Y.-F. Peng, "Adaptive intelligent backstepping longitudinal control of vehicleplatoons using output recurrent cerebellar model articulation controller," *Expert Syst. Appl.*, vol. 37, no. 3, pp. 2016–2027, Mar. 2010.

[8] Y.-N. Li, L. Zheng, Y. Hao, and J.-F. Liu, "Parameters self-tuning fuzzy-PID control on vehicle longitudinal control," *J. Jiangsu Univ. (Natural Sci. Ed.)*, vol. 27, no. 1, pp. 22–26, Jan. 2006.

[9] J. E. A. Dias, G. A. S. Pereira, and J. E. A. Dias, "Longitudinal model identification and velocity control of an autonomous car," *IEEE Trans. Intell. Transp. Syst.*, vol. 16, no. 2, pp. 776–786, Apr. 2015.

[10] C.-C. Tsai, S.-M. Hsieh, and C.-T. Chen, "Fuzzy longitudinal controller design and experimentation for adaptive cruise control and stop&go," *J. Intell. Robot. Syst.*, vol. 59, no. 2, pp. 167–189, Aug. 2010.

[11] G. J. L. Naus, J. Ploeg, M. J. G. Van de Molengraft, W. P. M. H. Heemels, and M. Steinbuch, "Design and implementation of parameterized adaptive cruise control: An explicit model predictive control approach," *Control Eng. Pract.*, vol. 18, no. 8, pp. 882–892, Aug. 2010.

[12] S. Li, F. Gao, K. Li, L.-Y. Wang, K. You, and D. Cao, "Robust longitudinal control of multi-vehicle systems—A distributed H-infinity method," *IEEE Trans. Intell. Transp. Syst.*, vol. 19, no. 9, pp. 2779–2788, Sep. 2018.

[13] J.-K. Liu and F.-C. Sun, "Research and development on theory and algorithms of sliding mode control," *Control Theory Appl.*, vol. 24, no. 3, pp. 407–418, Jun. 2007.

[14] G. D. Lee and S. W. Kim, "A longitudinal control system for a platoon of vehicles using a fuzzy-sliding mode algorithm," *Mechatronics*, vol. 12, no. 1, pp. 97–118, Feb. 2002.

[15] M. Jin, J. Lee, P. H. Chang, and C. Choi, "Practical nonsingular terminal sliding-mode control of robot manipulators for high-accuracy tracking control," *IEEE Trans. Ind. Electron.*, vol. 56, no. 9, pp. 3593–3601, Sep. 2009.

[16] E. Mousavinejad, Q.-L. Han, F. Yang, Y. Zhu, and L. Vlacic, "Integrated control of ground vehicles dynamics via advanced terminal sliding mode control," *Vehicle Syst. Dyn.*, vol. 55, no. 2, pp. 268–294, Feb. 2017.

[17] R. Mohammadi Asl, Y. Shabbouei Hagh, and R. Palm, "Robust control by adaptive non-singular terminal sliding mode," *Eng. Appl. Artif. Intell.*, vol. 59, pp. 205–217, Mar. 2017.

[18] L. Cao, X. Li, X. Chen, and Y. Zhao, "Minimum sliding mode error feedback control for fault tolerant small satellite attitude control," *Adv. Space Res.*, vol. 53, no. 2, pp. 309–324, Jan. 2014.

[19] Z. Yang, D. Zhang, X. Sun, W. Sun, and L. Chen, "Nonsingular fast terminal sliding mode control for a bearingless induction motor," *IEEE Access.*, vol. 5, pp. 16656–16664, Aug. 2017.

[20] Z. Sun, J. Zheng, H. Wang, and Z. Man, "Adaptive fast non-singular terminal sliding mode control for a vehicle steer-by-wire system," *IET Control Theory Appl.*, vol. 11, no. 8, pp. 1245–1254, May 2017.

[21] J. Guo, Y. Luo, and K. Li, "Adaptive neural-network sliding mode cascade architecture of longitudinal tracking control for unmanned vehicles," *Nonlinear Dyn.*, vol. 87, no. 4, pp. 2497–2510, Mar. 2017.

[22] H. S. Zad, T. I. Khan, and I. Lazoglu, "Design and adaptive sliding-mode control of hybrid magnetic bearings," *IEEE Trans. Ind. Electron.*, vol. 65, no. 3, pp. 2537–2547, Mar. 2017.

[23] P. Hang, X. Chen, B. Zhang, and T. Tang, "Longitudinal velocity tracking control of a 4WID electric vehicle," in *Proc. 5th Int.-Fed.-Autom.-Control (IFAC) Conf. Engine Powertrain Control, Simulation Modeling (E-COSM)*, Changchun, China, Sep. 2018, pp. 790–795.

[24] M. Zhu, H. Chen, and G. Xiong, "A model predictive speed tracking control approach for autonomous ground vehicles," *Mech. Syst. Signal Process.*, vol. 87, pp. 138–152, Mar. 2017.

[25] F. J. Lin and P. H. Shen, "Robust fuzzy neural network sliding-mode control for two-axis motion control system," *IEEE Trans. Ind. Electron.*, vol. 53, no. 4, pp. 1209–1225, Jun. 2006.

[26] X. Sun, H. Zhang, Y. Cai, S. Wang, and L. Chen, "Hybrid modeling and predictive control of intelligent vehicle longitudinal velocity considering nonlinear tire dynamics," *Nonlinear Dyn.*, vol. 97, no. 2, pp. 1051–1066, Jul. 2019.

[27] H. Jiang, F. Cao, and W. Zhu, "Control method of intelligent vehicles cluster motion based on SMC," *J. Jiangsu Univ. (Natural Sci. Ed.)*, vol. 39, no. 4, pp. 385–390, Jul. 2018.

[28] J. Xie, H. Jiang, and S. Ma, "Analysis on adaptive preview time of intelligent vehicle driver model," *J. Jiangsu Univ. (Natural Sci. Ed.)*, vol. 39, no. 3, pp. 254–259, May 2018.

[29] X.-Q. Sun, Y.-F. Cai, C.-C. Yuan, S.-H. Wang, and L. Chen, "Fuzzy sliding mode control for the vehicle height and leveling adjustment system of an electronic air suspension," *Chin. J. Mech. Eng.*, vol. 31, no. 25, Apr. 2018, Art. no. 35.

[30] H. Wang, K. Xu, Y. Cai, and L. Chen, "Trajectory planning for lane changing of intelligent vehicles under multiple operating conditions," *J. Jiangsu Univ. (Natural Sci. Ed.)*, vol. 40, no. 3, pp. 255–260, May 2019.

[31] L.-L. Wu, J.-H. Yang, R.-C. Wang, Q. Ye, and Z.-Y. Sun, "Global path planning for intelligent vehicles based on hybrid SA algorithm," *J. Jiangsu Univ. (Natural Sci. Ed.)*, vol. 40, no. 3, pp. 249–254, May 2019.

[32] C. Yin, H. Jiang, B. Tang, C. Zhu, Z. Lin, and Y. Yin, "Handling stability and energy-saving of commercial vehicle electronically controlled hybrid power steering system," *J. Jiangsu Univ. (Natural Sci. Ed.)*, vol. 40, no. 3, pp. 269–275, May 2019.

[33] X. Sun, C. Yuan, Y. Cai, S. Wang, and L. Chen, "Model predictive control of an air suspension system with damping multi-mode switching damper based on hybrid model," *Mech. Syst. Signal Process.*, vol. 94, pp. 94–110, Sep. 2017.

[34] R. Kianfar, B. Augusto, and A. Ebadighajari, "Design and experimental validation of a cooperative driving system in the grand cooperative driving challenge," *IEEE Trans. Intell. Transp. Syst.*, vol. 13, no. 3, pp. 994–1007, Sep. 2012.

[35] S. Li, K. Li, and J. Wang, "Economy-oriented vehicle adaptive cruise control with coordinating multiple objectives function," *Vehicle Syst. Dyn.*, vol. 51, no. 1, pp. 1–17, Aug. 2012.

[36] X. Fan, P. D. Walker, and Q. Wang, "Modeling and simulation of longitudinal dynamics coupled with clutch engagement dynamics for ground vehicles," *Multibody Syst. Dyn.*, vol. 43, no. 2, pp. 153–174, Jun. 2018.

[37] W. U. N. Fernando and S. Kumarawadu, "Discrete-time neuroadaptive control using dynamic state feedback with application to vehicle motion control for intelligent vehicle highway systems," *IET Control Theory Appl.*, vol. 4, no. 8, pp. 1465–1477, Aug. 2009.

[38] A. Fritz and W. Schiehlen, "Automatic cruise control of a mechatronically steered vehicle convoy," *Vehicle Syst. Dyn*, vol. 32, no. 4, pp. 331–344, 1999.

[39] X.-Y. Lu, J. Wang, S. E. Li, and Y. Zheng, "Multiple-vehicle longitudinal collision mitigation by coordinated brake control," *Math. Problems Eng.*, vol. 2014, Sep. 2014, Art. no. 192175.

SHAOHUA WANG received the Ph.D. degree in automotive engineering from Jiangsu University, Zhenjiang, China, in 2013. He is currently an Associate Professor with the School of Automotive and Traffic Engineering, Jiangsu University. His main research interests include energy management control of hybrid electric vehicles, control theory of hybrid systems, and control of electronically-controlled air suspension.

YIJIA HUI received the bachelor's degree in automotive engineering from Jiangsu University, Zhenjiang, China, in June 2015, where he is currently pursuing the master's degree in automotive engineering. His research interest includes longitudinal dynamic of intelligent vehicle.

XIAOQIANG SUN received the Ph.D. degree in automotive engineering from Jiangsu University, Zhenjiang, China, in June 2016. He is currently an Associate Professor with the Automotive Engineering Research Institute, Jiangsu University. His research interests include control of intelligent automobile and control of vehicle system dynamics.

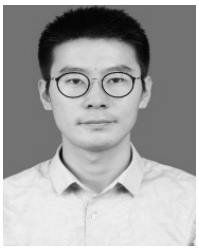

DEHUA SHI received the Ph.D. degree in automotive engineering from Jiangsu University, Zhenjiang, China, in June 2017. He is currently a College Lecturer in automotive engineering with Jiangsu University. His research interests include energy management control of hybrid electric vehicles and simulation and control of vehicle system dynamics.